

# Boron Phosphide Protective Coatings for Hazardous Radioactive Waste and Geothermal Power Applications

A.A. Ogwu<sup>1,\*</sup> and T. Hellwig<sup>1,2</sup>

<sup>1</sup> Thin Film Centre, School of Engineering, University of the West of Scotland, High Street, Paisley PA1 2BE, Scotland, U.K

<sup>2</sup> Now with P2i Ltd, Abingdon, Oxford OX1 4SA, England, U.K.

\*E-mail: [abraham.ogwu@uws.ac.uk](mailto:abraham.ogwu@uws.ac.uk)

Received: 10 June 2014 / Accepted: 19 September 2014 / Published: 28 October 2014

---

We investigated the corrosion susceptibility of Boron phosphide (BP) films deposited on stainless steel substrates by the plasma enhanced chemical vapour deposition (PECVD) process, when exposed to concentrated brine solution. The BP films were characterized with the scanning electron microscope (SEM), atomic force microscope (AFM), x-ray photoelectron spectroscopy (XPS) and Fourier transform Infra-red measurements (FTIR). The corrosion investigation involved open circuit potential (OCP) measurements for 20 hours, Potentiodynamic polarization and electrochemical impedance Spectroscopy (EIS) measurements. We also evaluated the role of the polar/dispersive components of the surface energy of the films on the corrosion process. The relationship between the polar component of the surface energy, the electric surface potential  $\psi$ , obtained through the Poisson-Boltzmann equation using the Debye-Huckel approximation and the double layer capacitance, all related through the Zeta potential is used to explain the improved corrosion resistance of the BP films. This creates an opportunity to prepare tailor-made corrosion resistant films during plasma processing. The results of our investigation indicates that the BP coatings could provide substantial additional corrosion protection for stainless steels, when used in extreme application areas like hazardous radioactive waste containers and geothermal brine containing environments against chloride attack.

---

**Keywords:** Boron Phosphide, Thin films, Surface energy, Corrosion, Radioactive waste, Electrochemistry

## 1. INTRODUCTION

Stainless steels for radioactive waste containers have to be exposed to extreme conditions including saturated brine containing environments, such as those proposed in the German radioactive waste disposal concept [ 1, 2]. This process involves containing the spent fuel in stainless steel

canisters and embedding them as waste packages in a rock salt formation. Loida et al [1] have simulated the corrosion challenges in such environments by studying the corrosion of steel materials used for this application in almost saturated,  $5.6 \text{ mol (Kg H}_2\text{O)}^{-1}$ , NaCl solution. Earlier work on the corrosion of steels used in radioactive waste containers exposed to  $5 \text{ mol Kg}^{-1}$  NaCl solution for 30 days was reported by Gimenez et al [3]. All of the above investigators have reported observing severe localised pitting chloride driven corrosion attack in the steels used for their investigations. Mundhenk et al [4,5] also investigated the corrosion stability of various steels, including stainless steels in geothermal brine environments. They observed localized corrosion in the steels, when the chloride concentration in the brine exceeded a certain limit around 50g/L of chloride brine. The least corrosion was observed for a nickel based alloy. They have proposed future trials involving polymer coatings for protecting steels when used in geothermal brine containing environments such as heat exchangers, pumps, tubes e.t.c Pfenning et al [6] have also investigated the corrosion and corrosion fatigue of high alloy steels for applications in environments containing saturated brine solutions, including geothermal engineering, oil and gas exploration and carbon capture and storage [ CCS], where corrosion and mechanical stress have a combined role and observed severe chloride attack. The development of corrosion resistant protective surface coatings, based on polymers and ceramic materials, to protect stainless steels from severe chloride attack leading to localised pitting corrosion is a current major on-going research activity in areas as diverse as marine applications, molten carbonate fuel cell technology and biomaterial implants [7,8].

There have been earlier attempts in the literature to find protective coatings for improving the corrosion performance of steels and stainless steels used in geothermal power-plants, where they are exposed to acid-brine steam. Sugama [9] reported attempts to adopt titanium carbo-nitride coatings as corrosion protection barriers for steels used in geothermal power plants.

Boron Phosphide (BP) has been previously investigated for its tribological and engineering promise in protecting aerospace and marine infra-red optics [10, 11].

In the present work, we report our investigation on the scientific basis of the corrosion resistance of BP coated, compared uncoated stainless steel substrates, when exposed to an extreme environment like concentrated brine solution, which occurs in hazardous radioactive waste containers and in geothermal power generation plants. The scientific explanation is based on our new unpublished detailed electrochemical impedance spectroscopy (EIS) measurements reported in this paper. This is the first of such investigation on BP coatings in the literature to the best knowledge of the present authors.

The relationship between the polar component of the surface energy and the double layer capacitance, through the Zeta potential is used to explain the improved corrosion resistance at a certain composition of the films. Our approach explores the relationship between the surface forces contained within the extended Derjaguin-Landau-Verwey-Overbeek (XDLVO) theory and the electric surface potential  $\psi$  of the electrical double layer formed between the BP surface and saturated brine, within the Gouy-Chapman diffuse layer model. The Poisson-Boltzmann equation containing the surface potential  $\psi$  can be solved to determine the electrical double layer interaction energy, which then leads to the double layer capacitance. This relationship creates the opportunity to use changes in the polar component of the surface energy, carried out during the plasma processing of the BP coatings to

induce changes in the double layer capacitance of the surface of the BP when exposed to brine solution, since they are both connected through the Zeta potential as shown in this paper. This creates an opportunity to prepare tailor-made corrosion resistant films through this understanding for many other areas of application..

The BP coated and as received polished stainless steel plates were tested for corrosion degradation in a 5.7 molar ( $5.7 \text{ mol/dm}^3$ ), NaCl aqueous solution at  $25^\circ\text{C}$  respectively. Such a highly concentrated saline solution was used to simulate a severe case of chloride attack, as occurs in extreme environments like in containers for hazardous radioactive waste exposed to repositories containing rock salt formation or in geothermal power plants or other extreme chloride containing conditions [1, 2, 3]. This paper is also focussed on investigating any possible underlying role that surface energies might have on the corrosion of Boron phosphide films in aqueous environments [12-16].

## 2. EXPERIMENTAL INVESTIGATION

### 2.1 Film Deposition:

The BP films were prepared by a Nordiko PECVD facility located at Thales Optronics, Glasgow, Scotland, U.K. The precursors gases used for the deposition on stainless steel and ZnS substrates were diborane ( $\text{B}_2\text{H}_6$ ) and phosphine ( $\text{PH}_3$ ), diluted in hydrogen gas, which served as the carrier gas. Argon gas was used to initiate and maintain the plasma during the deposition process at an rf frequency of 13.56MHz.

**Table 1.** The composition of the as-received 304L stainless steel substrates used for the deposition of the Boron phosphide coatings.

Steel type	Carbon (wt %)	Nickel (wt %)	Chromium (wt %)	Manganese (wt %)	Silicon (wt %)	Nitrogen (wt %)	Iron (wt%)
304L	0.03 max	8-12.0	18-20.0	2.0 max	0.75 max	0.10 max	Balance

**Table 2.** The gas flow rates used during the deposition of the Boron phosphide coatings.

Diborane flow rate ( $\text{cm}^3/\text{min}$ )	Phosphine flow rate ( $\text{cm}^3/\text{min}$ )	Ratio $\text{PH}_3/\text{B}_2\text{H}_6$
15	55	3.7
15	60	4.0
15	65	4.3
15	70	4.7
15	75	5.0
15	80	5.3
15	85	5.7
15	90	6.0

The composition of the as-received steel sample is as indicated in Table 1. The chamber pressure was maintained at 30mTorr and the substrate temperature during deposition was 350°C. The gas flow rate was measured in standard cubic centimetres per minute (cm<sup>3</sup>/min). The diborane flow rate was held at 15cm<sup>3</sup>/min, whilst the phosphine flow rate was varied from 55 cm<sup>3</sup>/min to 90 cm<sup>3</sup>/min in 5cm<sup>3</sup>/min increments. The flow rates of the gases during deposition are as indicated in Table 2.

### 2.2 SEM /AFM investigation

A Hitachi S- 4100 SEM was used for the examination of the BP films at magnifications that ranged between 20X and 5,000X. A combined AFM and Nano-indenter, Nanoscope III scanning probe microscope manufactured by Digital instruments was used for further surface characterisation. A more detailed view is given by atomic force microscopy of the BP films prepared at different phosphine flow rates during deposition as shown in fig.1.

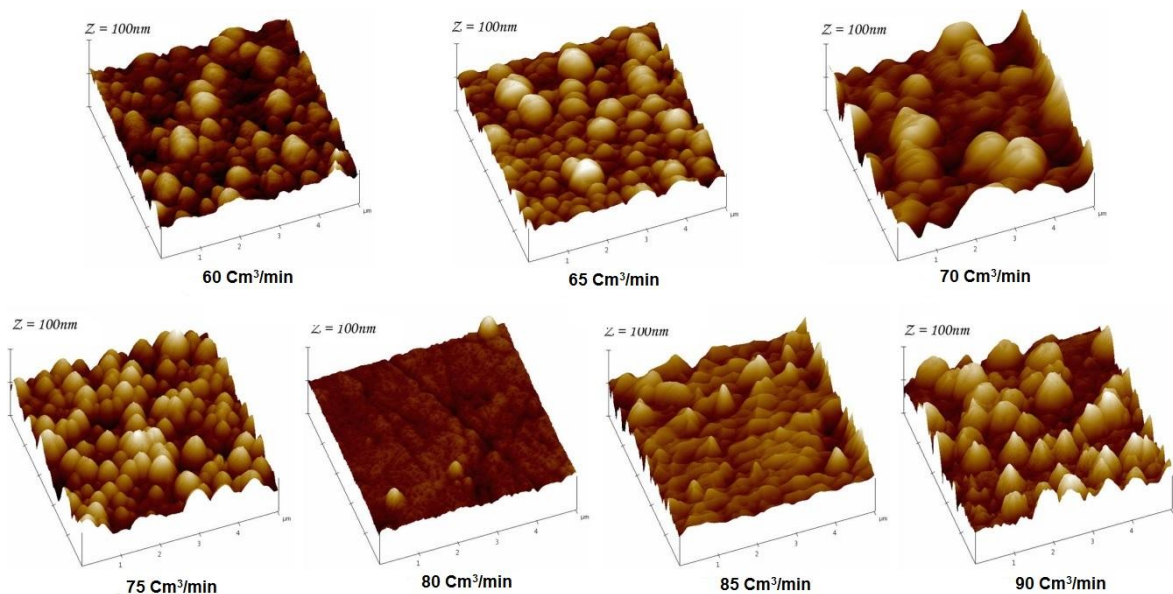


**Figure 1.** AFM images of the BP surfaces at different PH3 flow rates. These images are representative of the AFM surface images of films deposited between 60 and 90 cm<sup>3</sup>/min phosphine flow rates.

### 2.3 FTIR Film Thickness measurement

The thickness of the films was measured by observing interference fringe pattern maxima in the reflectance spectra in the infra-red of the deposited BP films using an IR spectrometer. The thickness (t) of the films can be expressed as [17],

$$t = \frac{N}{2(\lambda_1 - \lambda_2) \cdot n} \tag{1}$$

Where,  $\lambda_1$  and  $\lambda_2$  are the initial and final wavelengths,  $n$  is the refractive index and  $N$  is the number of fringes between  $\lambda_1$  and  $\lambda_2$ . The average values of ten separate measurements of the thicknesses of the films are summarised in Table 3.

**Table 3.** The calculated thicknesses for the different compositions of the deposited BP films

PH <sub>3</sub> [cm <sup>3</sup> /min]	Thickness [μm]
60	7.1
70	9.3
80	9.5
90	9.7

#### 2.4 X-ray photoelectron spectroscopy (XPS).

**Table 4.** Relative % atomic concentration and binding energies – BP films.

PH <sub>3</sub> [cm <sup>3</sup> /min]	B1s B.E.	B		P2p B.E.	P		P:B	
		at.%	wt.%		at. %	wt. %	at.%	wt.%
60	187.8	36	16	130.0	64	94	1.78	3.9
75	187.9	47	24	130.1	53	94	1.13	4.0
90	187.9	48	24	129.9	52	93	1.08	5.6

XPS investigation was carried out with a VG Escalab 200D spectrometer with a HSA analyser. Mg K<sub>α</sub> x-ray was used for the excitation at energy of 15KeV and an emission current of 20 mA. The elemental sensitivity was about 0.1atomic % and the pressure during the examination was better than  $8 \times 10^{-10}$  mbar. The results of the XPS investigation on the prepared films are summarised in Table 4. All of the BP films investigated were found to be non-stoichiometric, with a B/P ratio greater than one.

#### 2.5 Surface energy measurements

The contact angle measurement was conducted with a CAM 200 goniometer manufactured by KSV Ltd of Finland to obtain the surface energy. Three liquids namely water; ethylene glycol and Diiodomethane were used for the measurements. The surface energy values were calculated by both the Fowkes, Owens and Wendt geometric mean approach (GME) and the Lifshitz- Van der Waals acid-base approach (LWAB) [18].

### 3. THEORY

#### 3.1 Surface energy / Contact angle:

According to the classical Derjaguin-Landau-Verwey-Overbeek (DLVO) theory, the interaction between two bodies separated by a fluid is described by the sum of the attractive Lifshitz-

Van der Waals energy (LW) and an electrostatic energy (EL) due to an electric double layer [18-19]. For many uncharged materials the presence, of additional interactions has been observed [18-19]. This has led to the proposal of the extended DLVO or XDLVO theory [18-19], to account for the additional interactions. The additional contribution in the XDLVO theory is the contribution from short ranged acid-base (AB) interactions. This electron donor/ electron acceptor interaction may be hydrophobic or hydrophilic. The XDLVO total free energy of interaction or adhesion on a solid can be expressed as

$$\Delta G_{total} = \Delta G_{EL} + \Delta G_{LW} + \Delta G_{AB} \text{-----} (2)$$

$\Delta G_{EL}$ ,  $\Delta G_{LW}$ , and  $\Delta G_{AB}$ , are contributions from the Electrostatic, Lifshitz – Van der Waals, and Acid-Base energy terms to the total interaction energy. The electrostatic interaction energy per unit area between two infinite planar surfaces separated by a fluid is given by

$$\Delta G_{EL} = \frac{\epsilon_0 \epsilon_i \kappa}{2 (\zeta_i^2 + \zeta_j^2)} \text{-----} (3)$$

$\epsilon_0 \epsilon_i$  is the dielectric permittivity of the suspending fluid,  $\kappa$  is the inverse Debye screening length,  $\zeta_i$  and  $\zeta_j$  are the surface potentials of the interacting solids i and j.

This surface potential is determined by Zeta potential measurements. For uncharged interacting surfaces, the free energy of adhesion is written as

$$\Delta G_{total} = \Delta G_{LW} + \Delta G_{AB} \text{-----} (4)$$

$\Delta G_{LW}$ ,  $\Delta G_{AB}$  and  $\Delta G_{total}$  can be determined once the surface energy terms are known. These surface energy terms are derived using two approaches, namely the geometric mean approach proposed by Fowkes [20] and by Owens and Wendt [21], and the acid-base approach developed by Van Oss et al [22]. In the Fowkes [20] approach the total surface energy ( $\gamma$ ) of a material can be expressed as:

$$\gamma = \gamma^p + \gamma^d \text{-----} (5)$$

$\gamma^p$  is the Polar component of the Surface energy

$\gamma^d$  is the Dispersive component of the Surface energy

The polar interaction term consists mainly of

- (i) dipole – dipole interactions
- (ii) dipole – induced dipole interactions

The dispersive energy term is predominantly made up of the London dispersion energy.

The interfacial tension between two bodies labelled i and j can also be written in the form:

$$\gamma_{ij} = \gamma_i + \gamma_j - 2\phi^d - 2\phi^p \text{-----} (6)$$

$\phi^d$  = dispersive interaction term

$\phi^p$  = polar interactive term

### 3.2 Polar term

The polar interaction term  $\phi^p$  in equation (6) can be approximated by

$$\phi^p = (\gamma_i^p \gamma_j^p)^{1/2} \text{-----} (7)$$

as suggested by Fowkes [20] and Wu [23]

### 3.3 The dispersion term

It has been argued that the dispersion energy term can be approximated using the geometric mean approximation in equation (7) i.e.

$$\phi^d \sim (\gamma_i^d \gamma_j^d)^{1/2} \quad (8)$$

This leads to two expressions generally applied to determine the surface energy of two interacting phases and in the case of a solid and a liquid will be

$$\gamma_{SL} = \gamma_S + \gamma_L - 2(\gamma_L^p \gamma_S^p)^{1/2} - 2(\gamma_L^d \gamma_S^d)^{1/2} \quad (9)$$

Owen and Wendt applied the Young – Dupre equation

$$\gamma_L \cos\theta = \gamma_S - \gamma_{SL} \quad (10)$$

to the Fowkes expression for interfacial energy in equation (9) to

obtain an equation of a straight line in the form of  $Y=Mx + C$ , and  $\gamma_S^p = M$  and  $\gamma_s^d = C$ , determined using contact angle ( $\theta$ ) measurement from a range of liquids. Another approach is the Lifshitz-Van der Waals / Acid-base approach also called the Van Oss-Chaudhry-Good approach [22].

The total surface energy of a surface is represented as

$$\gamma = \gamma^{lw} + \gamma^{AB} \quad (11)$$

where  $\gamma^{lw}$  is the non-polar electrodynamic component consisting of contributions from the London, Debye and Keesom dipole interactions and  $\gamma^{AB}$  is the acid-base component of the surface energy, mainly due to hydrogen bonding and split into two non-additive electron acceptor ( $\gamma^+$ ) / electron donor ( $\gamma^-$ ) parameters expressed as

$$\gamma^{AB} = 2 (\gamma^+ \gamma^-)^{1/2} \quad (12)$$

The measurement of the contact angle of three liquids with known values of  $\gamma^{lw}$ ,  $\gamma^+$  and  $\gamma^-$  is required to determine the surface energy in this case.

### 3.4 Corrosion and Electrochemical Impedance Measurement.

A Volta lab, 40 consisting of a PGZ 301 potentiostat and a CCTO electro-chemical cell, was used for the corrosion test. The three electrode cell had a stainless steel counter electrode and a Standard Calomel reference electrode. All of the corrosion measurements reported in this paper, are measured relative to the standard calomel electrode (SCE). The working electrode was the sample surface. The working electrode area was 40cm<sup>2</sup>. The Voltmaster 4 software was used for processing the results of the electrochemical measurement. Open circuit potential measurements were carried out on the samples, followed by potentiodynamic polarisation investigation. The applied potential was used to polarise the sample from -1000mV vs SCE to +3000 mV vs SCE at a scan rate of 0.32mV/s. The electrochemical impedance spectroscopy (EIS) measurement was performed at a frequency range from 10<sup>-3</sup> to 10<sup>5</sup> Hz and AC amplitude of 20mV. The BP coated and as received polished stainless steel plates were tested for corrosion degradation in a 5.7 molar (5.7 mol/dm<sup>3</sup>), NaCl aqueous solution at 25°C respectively. Such a highly concentrated saline solution was used to simulate a severe case of chloride attack.

### 4. EXPERIMENTAL RESULTS

The results of the contact angle measurements on the BP films for the three liquids are shown in Fig.2.

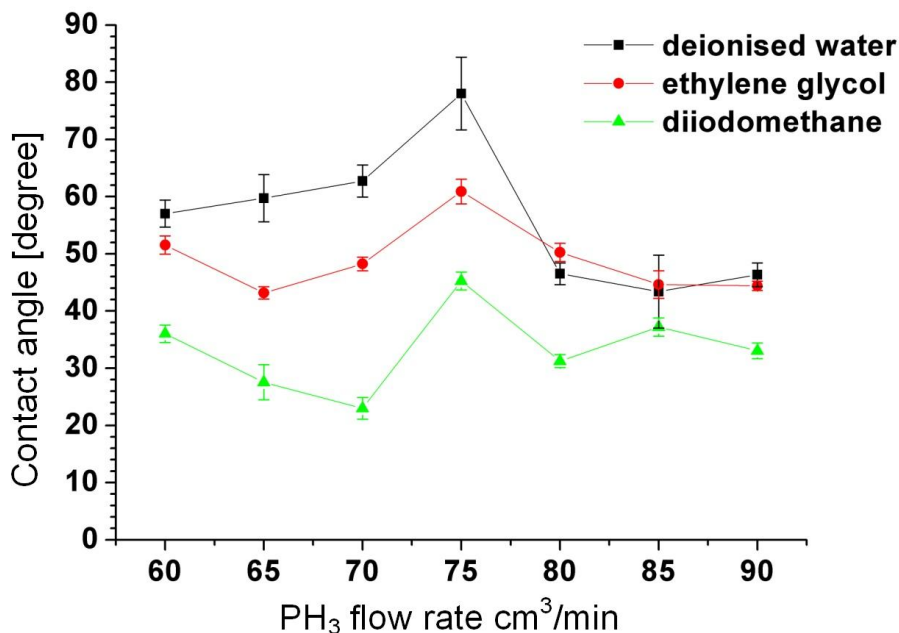


**Figure 2.** Contact angles of three liquids on boron phosphide films prepared at various phosphine flow rates during deposition.

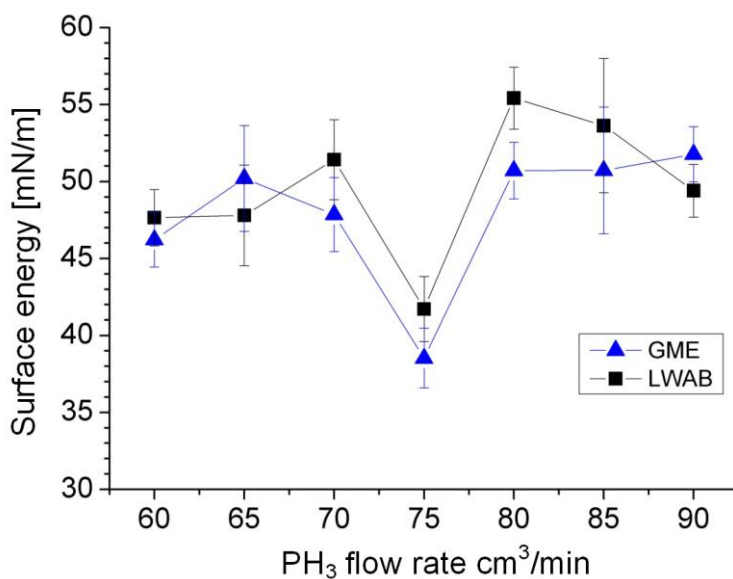


**Figure 3.** Surface free energy of boron phosphide films prepared at various phosphine flow rates during deposition measured by the Fowkes, Wu and Acid-Base approach.

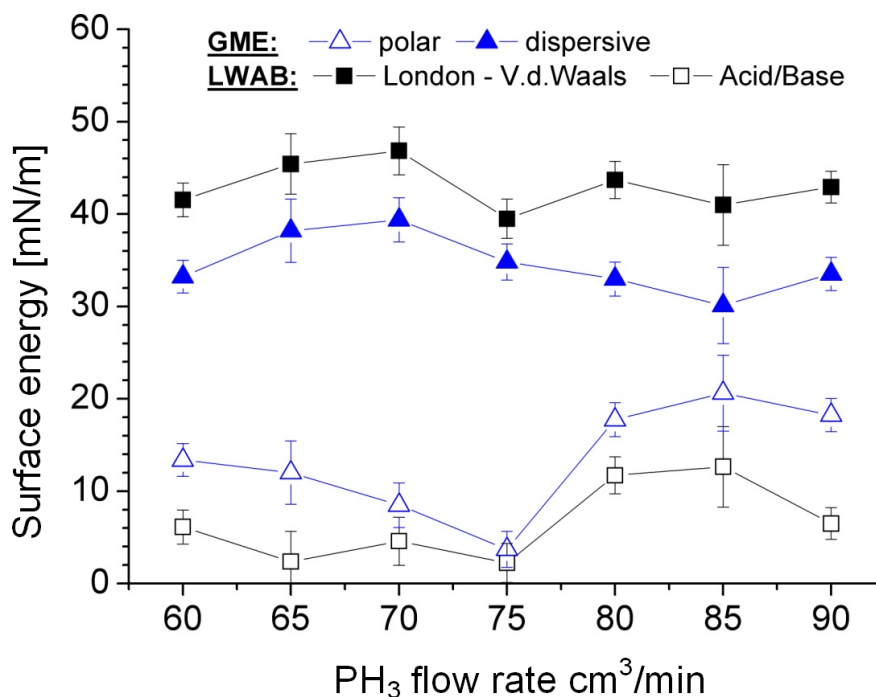


**Figure 4.** Breakdown of the dispersive and polar component of the Wu surface energy measurement for the various compositions of the Boron Phosphide (BP) films investigated.

The highest contact angle with water of 80 degrees was obtained for the film prepared at 75 cm<sup>3</sup>/min phosphine flow rate. The results of the surface energy measurements using the Fowkes geometric mean approach of Owens and Wendt, the Wu and the Acid-Base approach are shown in Fig.3 and the polar and dispersive components of the Wu surface energy terms as shown in Fig.4. The highest contact angle with water obtained on the film prepared at 75 cm<sup>3</sup>/min phosphine flow rate can be explained in terms of the small value of the polar component of the surface energy of the films. The water contact angle variation with phosphine flow rate during deposition also indicates that the contact angle and surface energy of BP films can be varied to suit specific applications.

#### 4.1 OCP measurement:

A typical behaviour of the stainless steel under open circuit conditions compared to the BP coated stainless steel is shown in Fig. 5 for the film prepared at 90 cm<sup>3</sup>/min PH<sub>3</sub> flow rate. A similar pattern was observed for all BP coated stainless steel samples examined with phosphine flow rates ranging from 60 to 90 cm<sup>3</sup>/min during deposition.

The open circuit potential (OCP) of the polished uncoated stainless steel was found to decrease steadily with time as shown in Fig. 5. The OCP decreased to a value of -50mV vs SCE after 20 hours. On many occasions during the OCP measurement on the uncoated steel sample, the value of the OCP

at various times decreased sharply and rose again as shown in Fig.5. This is believed to be due to the initial formation of a thin protective passivating oxide layer on the uncoated steel samples, with occasional dissolution and penetration of the passivating layer by chloride ions from the solution. The sharp rise in the OCP after this observed drop is suspected to be due to the formation of a re-passivating layer in the regions where the initial passivating layer would have broken down. All of the BP coated stainless steel plates regardless of their initial OCP became nobler with time, unlike the uncoated stainless steel plates, whose potential continued to decrease in value. After 20 hours of exposure to the saline solution, all of the BP coated samples had a higher OCP value than the uncoated polished steel samples. The more positive OCP potential on the BP coated steel samples and the absence of the regular sharp drop in OCP compared to the uncoated steel plates is an indication of the presence of a stable protective passivating layer on the BP coated substrates. This is an indication of the potential of BP films to act as a protective coating for stainless steels in a strong saline solution.

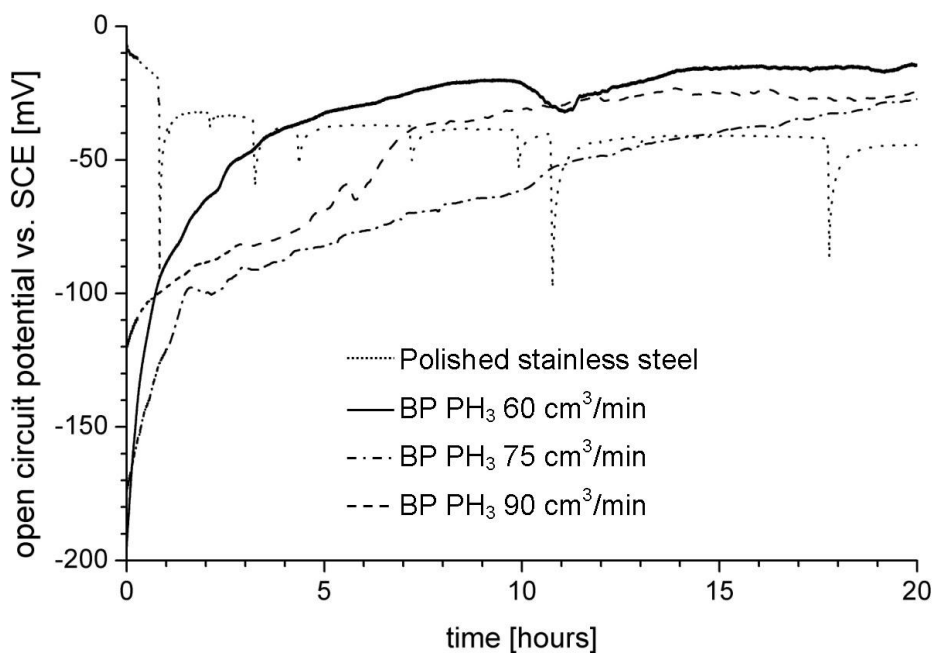


**Figure 5.** Open circuit potential measurements on the BP coated and uncoated stainless steel substrate.

#### 4.2 Tafel Plot and Potentiodynamic Polarization:

The combined potentiodynamic polarisation curve in the anodic region for both the coated and uncoated stainless steel plates is shown in Fig.6. As shown in Fig.6, the breakdown potential for a sharp current rise is 100mV vs SCE for the uncoated stainless steel plate, whilst the breakdown potential for the BP coated substrates containing BP films prepared between 75 and 80 cm<sup>3</sup>/min, phosphine flow rate was in excess of 2,500 mV vs SCE. This is another clear indication of the capability of BP films to protect stainless steel from corrosion in a saline solution. The Tafel plots were used to determine the corrosion potential, corrosion current, polarization resistance and corrosion rates of the BP coated and uncoated steel substrates.

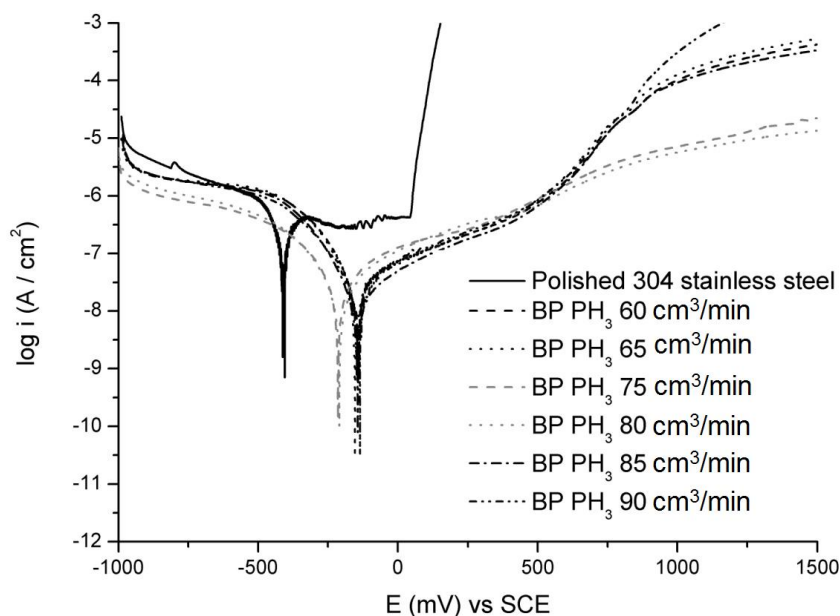


**Figure 6.** Potentiodynamic polarization curves of the BP coated and uncoated stainless steel substrates.

The uncoated stainless steel is again observed to have the lowest short term corrosion potential  $E_{corr}$  of - 415.5 mV vs SCE and the highest corrosion current  $i_{corr}$  of 192.4 nA/cm<sup>2</sup> as shown in Table 5. The uncoated steel substrate also had the least recorded value of polarization resistance.

**Table 5.** Corrosion potential, corrosion current and polarisation resistance values obtained for the BP coated and uncoated stainless steel substrates (304SS).

Sample	$E_{corr}$ (vs. SCE) mV	$R_p$ Slope $M\Omega cm^2$	$R_p$ $M\Omega$ $cm^2$	$i_{corr}$ $A/cm^2$ ( $\times 10^{-8}$ )	$\Delta i_{corr}$ $A/cm^2$ ( $\times 10^{-8}$ )	$\beta_a$ mV/decade	$\beta_c$ mV/decade	$C_R$ $\mu m/a$
60	-145.3	1.18	1.54	2.90	1.00	357.4	-144.0	0.6
65	-128.1	1.34	1.72	2.60	0.60	359.4	-140.6	0.6
75	-218.7	1.87	2.36	1.20	0.80	156.4	-116.2	0.3
80	-165.2	1.07	1.44	3.40	1.00	428.3	-151.5	0.8
85	-140.0	1.94	2.52	1.50	0.50	263.4	-128.8	0.4
90	-136.2	1.53	1.56	4.40	2.00	516.6	-229.7	1.0
304 SS	-415.5	0.12	0.18	192.4	4.00	255.4	-118.2	2.3

4.3 Electrochemical impedance spectroscopy (EIS).

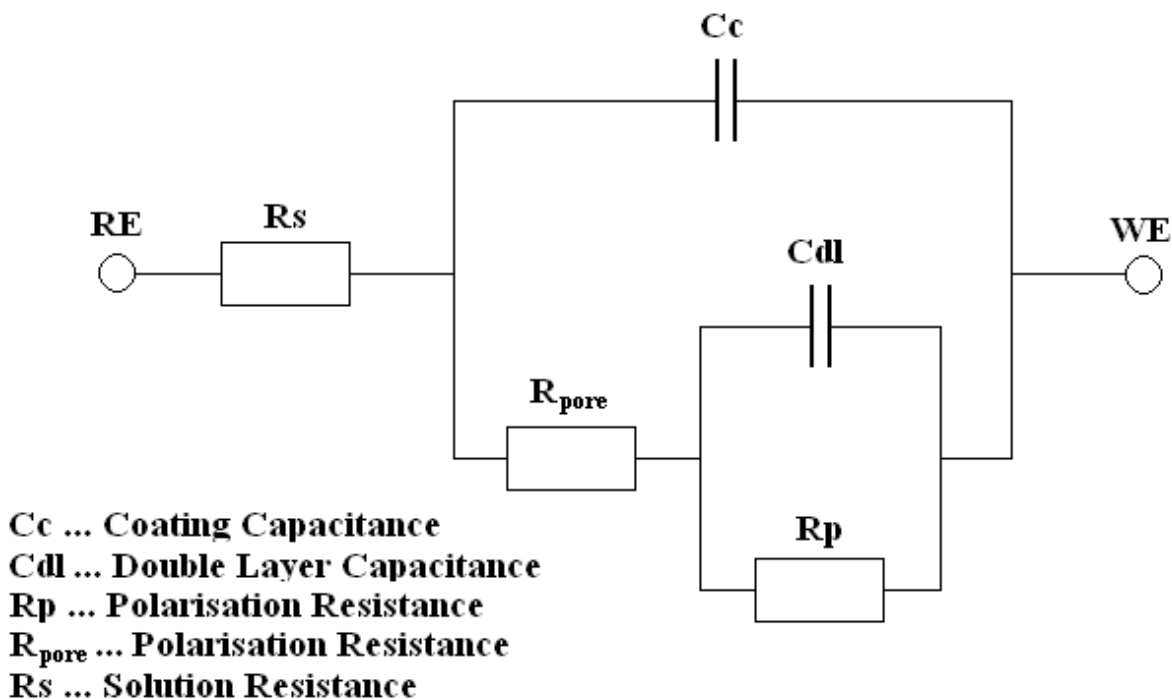


Figure 7. Equivalent circuit model for the tested BP films.

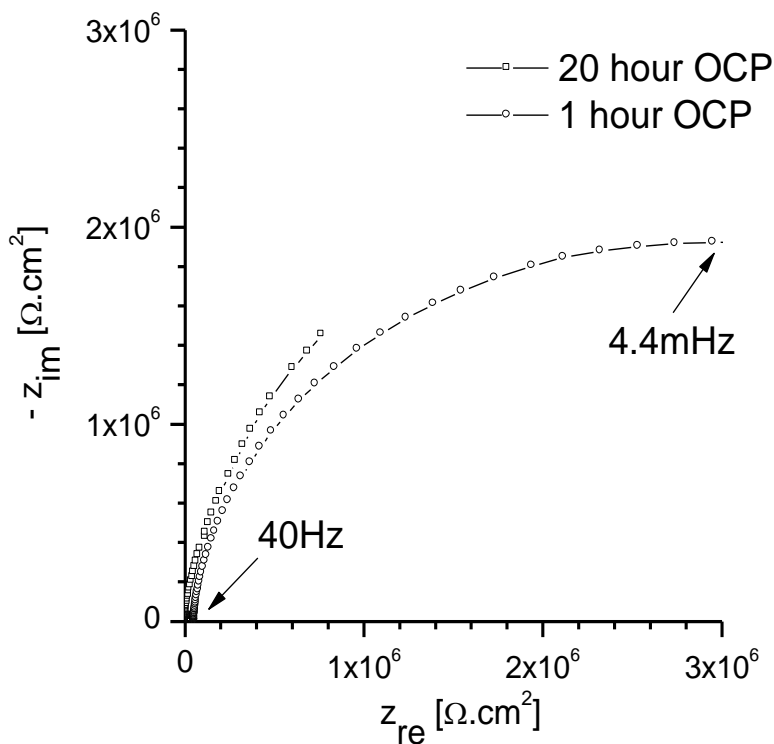
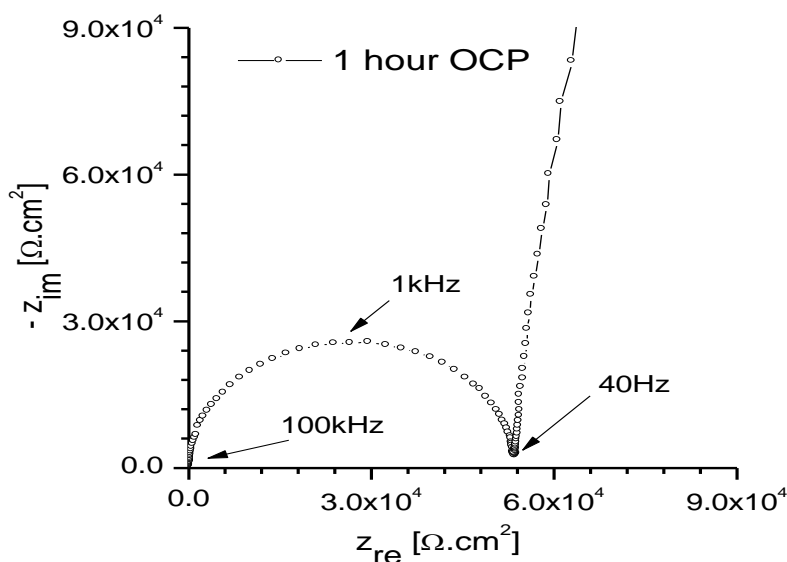
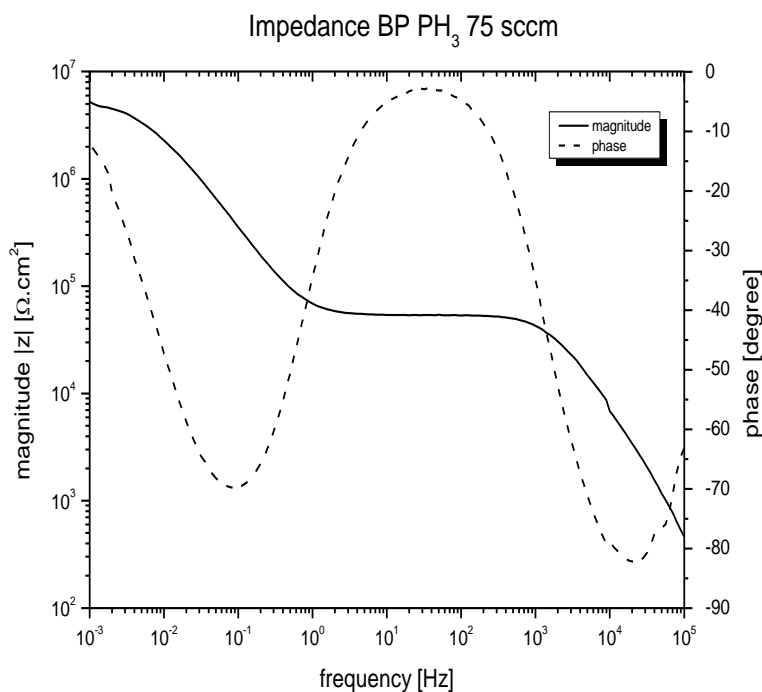


Figure 8. a) Section of the Nyquist plot from the EIS test on the BP coated steel substrate for the film prepared at 75 cm<sup>3</sup>/min phosphine flow rate after a 1 hour and 20hours exposure to open circuit conditions (OCP). The solution resistance (Rs) and the pore resistance (Rp) curve.



**Figure 8. b)** Pore resistance extracted from Nyquist plot from the EIS test on the BP coated steel substrate for the film prepared at 75 cm<sup>3</sup>/min phosphine flow rate shown in fig 8a, after 1 hour under open circuit conditions (OCP).



**Figure 8. c)** Bode plot from the EIS test on the BP coated steel substrate for the film prepared at 75 cm<sup>3</sup>/min phosphine flow rate shown in fig. 8a.

We recorded both the Nyquist and Bode plots of the investigated BP coated substrates, with saline solution as the electrolyte. An equivalent circuit consisting of  $R_s$ , the solution resistance of the electrolyte,  $R_{pore}$ , pore resistance,  $C_{dl}$ , the double layer capacitance of the coating and  $R_p$ , the

polarization resistance at the coating /substrate interface was used to fit the data as shown in Fig. 7. A typical Nyquist plot obtained from the film prepared at 75  $\text{cm}^3/\text{min}$  phosphine flow rate is shown in Fig .8a. The highest polarization resistance was obtained for the films deposited between 75 and 85  $\text{cm}^3/\text{min}$ , in agreement with the potentiodynamic polarization plots. The pore resistance from the Nyquist plot for 75  $\text{cm}^3/\text{min}$ , phosphine flow rate deposited film is shown in Fig. 8b and a Bode plot for the same film is shown in Fig.8c.

## 5. DISCUSSION

The large value of the corrosion current for the uncoated steel shown in Table 5, compared to the BP coated steels is believed to be due to both a barrier effect by the coating and a reduction in both the anodic and cathodic reactions during the corrosion process.

The basic anodic reaction on steels resulting in the dissolution of iron is given by [24],

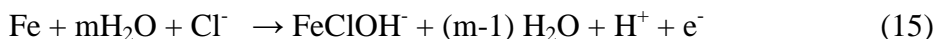


The cathodic reaction is,



The electrons produced at the anode are consumed at the cathode. The rate of the above reactions has been reported to be reduced by the addition of certain alloys to uncoated steel [24]. However as suggested by Qu et al [25], Sodium Chloride can accelerate both the anodic and cathodic reactions, based on the following reaction mechanisms.

Anodic reaction,



Cathodic reaction,



We expect the above proposed mechanism to be present in our uncoated steel sample, leading to the observed substantially high corrosion current as shown in Figs. 5 and 6 and in Table 5, due to the breakdown of the passive oxide. This believed to due to the attack of the uncoated steel surface by aggressive chloride ions. The BP coating is able to protect against this attack, leading to much lower values of corrosion currents, as explained here. Ohtsuka [26] has reported that the corrosion protection offered by conducting polymer coatings to steels, is due to the limited diffusion mobility of chloride

ions in conducting polymer coatings. We believe a similar mechanism operates in the BP coatings on the steels we investigated, with chloride ions having a very low diffusion mobility in the coatings. This will also lead to a reduction in the rates of both the anodic and cathodic reactions respectively.

The DLVO theory expresses the interaction energy between surfaces as the sum of interactions consisting of a Van der Waals attractive term ( $V_{vdw}$ ) and an electric double layer term ( $V_{EDL}$ ), which is usually repulsive, but becomes attractive when ions/surfaces of opposite charge are interacting, as already indicated in equations 2,3 and 4. This is the case during the electrochemical interaction of NaCl electrolyte solution with the Boron phosphide coatings as the working electrode under electrochemical testing conditions, where ions are attracted due to opposite polarity.

These interaction terms can be determined through the surface energy components, polar, dispersive and acid/base terms.

It can be shown that that,

$$V_{vdw} = - \frac{A}{12\pi x^2} \tag{17)}$$

A is the Hamaker constant,

x is the separation between two flat surfaces.

The Hamaker constant is directly related to the total surface energy ( $\gamma$ ) through the expression below [22], for two plane surfaces in a vacuum separated by a distance x,

$$A = 24 \pi x^2 \gamma \tag{18)}$$

$\gamma$  is the total surface energy.

The electric surface potential  $\psi$  of the electrical double layer within the Gouy-Chapman diffuse layer model can be solved to determine the electrical double layer interaction energy, by solving the Poisson-Boltzmann equation, which in the linearised form is expressed as [27],

$$\frac{d^2 \psi(x)}{dx^2} = \kappa^2 \psi(x) \tag{19)}$$

x is the distance and  $\kappa^{-1}$  is the Debye length.

It can be shown that the solution of the Poisson-Boltzmann equation, using the Debye-Huckel approximation [27], leads to a solution for the potential of a particle of radius  $R_a$  of the form,

$$V_{EDL} = 2 \pi R_a \zeta \exp(-\kappa x) \tag{20)}$$

$\zeta$  is the zeta potential.

The double layer capacitance ( $C_{dl}$ ) is expressed as

$$\frac{1}{C_{dl}} = \frac{1}{C_H} + \frac{1}{C_{diff}} \tag{21)}$$

$C_{diff}$  is the diffuse layer capacitance,

$C_H$  is the Helmholtz layer capacitance

Any change in the polar component of the surface energy ( $\gamma^p$ ) will lead to a change in the electrical double layer interaction potential, the zeta potential and the value of the double layer capacitance ( $C_{dl}$ ). This is supported by our experimental investigation, shown in Fig.9a, indicating that the lowest value of the double layer capacitance ( $C_{dl}$ ) of around  $5\mu F/cm^2$  occurs for films deposited at the same composition, i.e.  $75 \text{ cm}^3/\text{min}$  phosphine flow rate, where the highest contact angle with water and the lowest value of the polar component of the surface energy ( $\gamma^p$ ) was observed as shown in Figs. 2, 3 and 4.

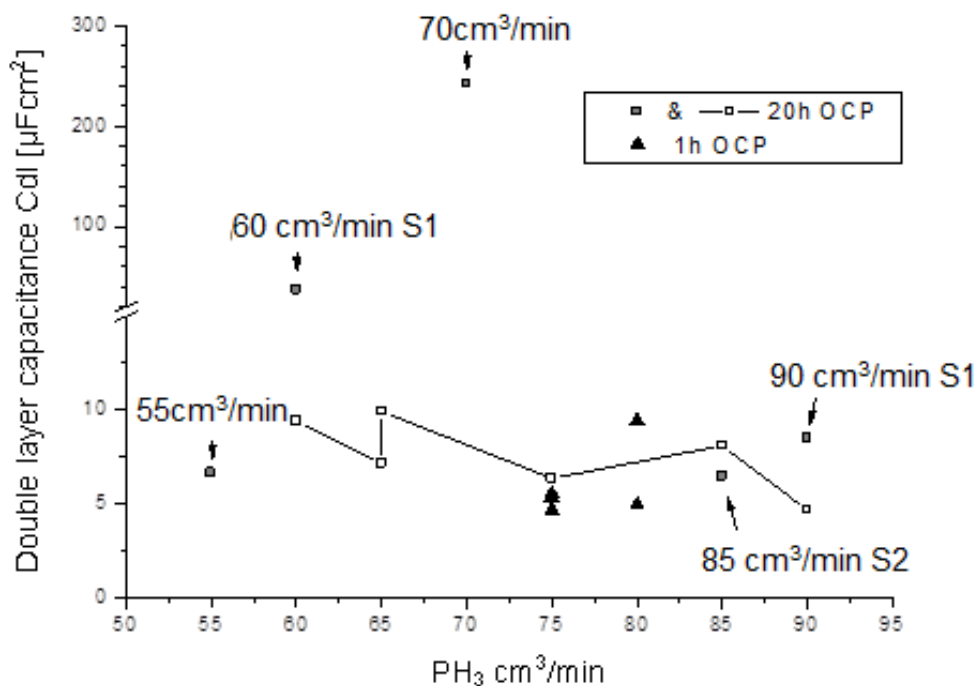


**Figure 9. a)** A plot of the variations of the double layer capacitance ( $C_{dl}$ ) of films immersed in 5.7M NaCl solution under OCP conditions for 1 hour and 20 hours before the EIS test was performed against phosphine flow rate during deposition.

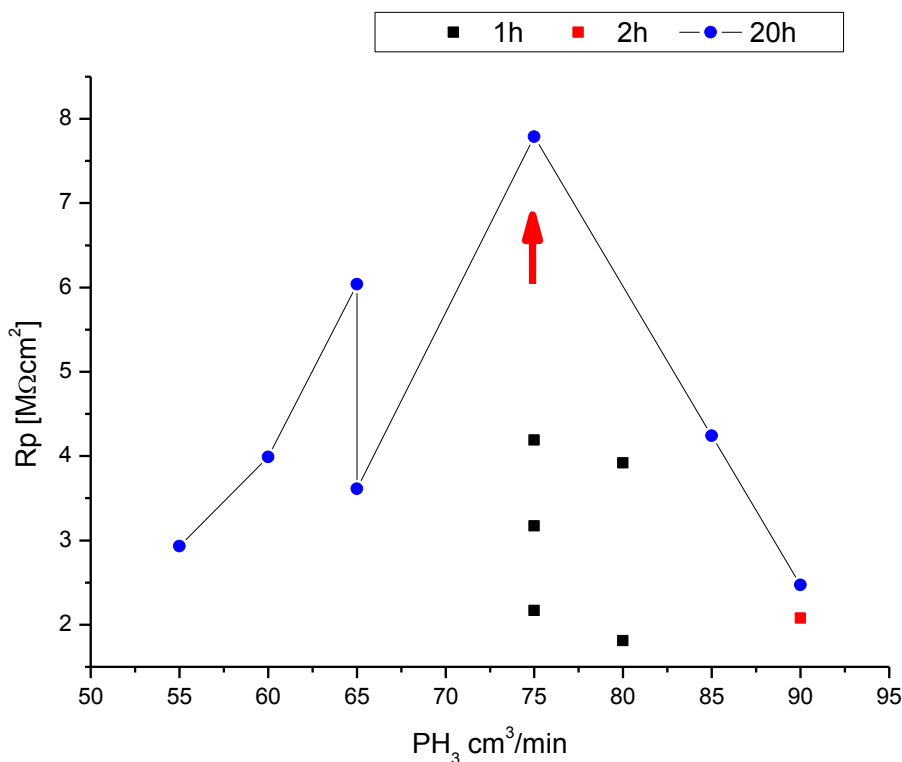


**Figure 9. b)** A plot of the variations in the polarization resistance of the films immersed in 5.7 M NaCl solution under OCP conditions for 1 hour, 2 hours and 20 hours before the EIS test was performed.

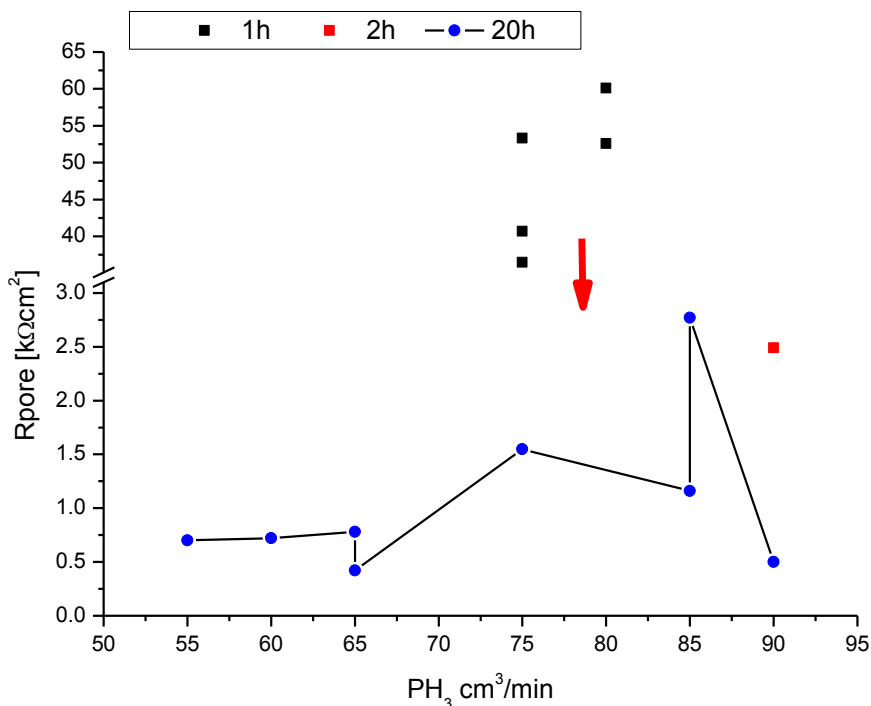


**Figure 9. c)** A plot of the variations in pore resistance of films immersed in 5.7 M NaCl solution under OCP conditions for 1 hour, 2 hours and 20 hours before the EIS test was performed against phosphine flow rate during deposition.

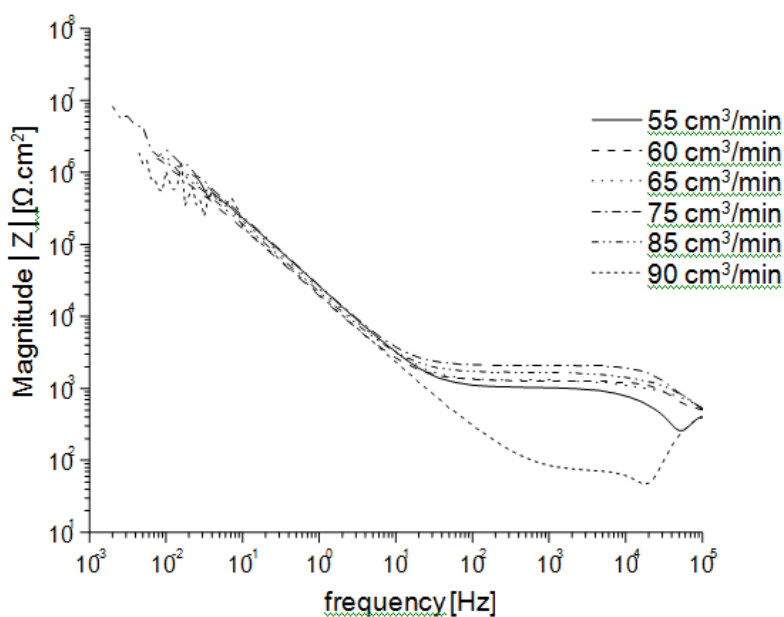


**Figure 10.** Bode plots obtained for the BP coated stainless steel substrates.

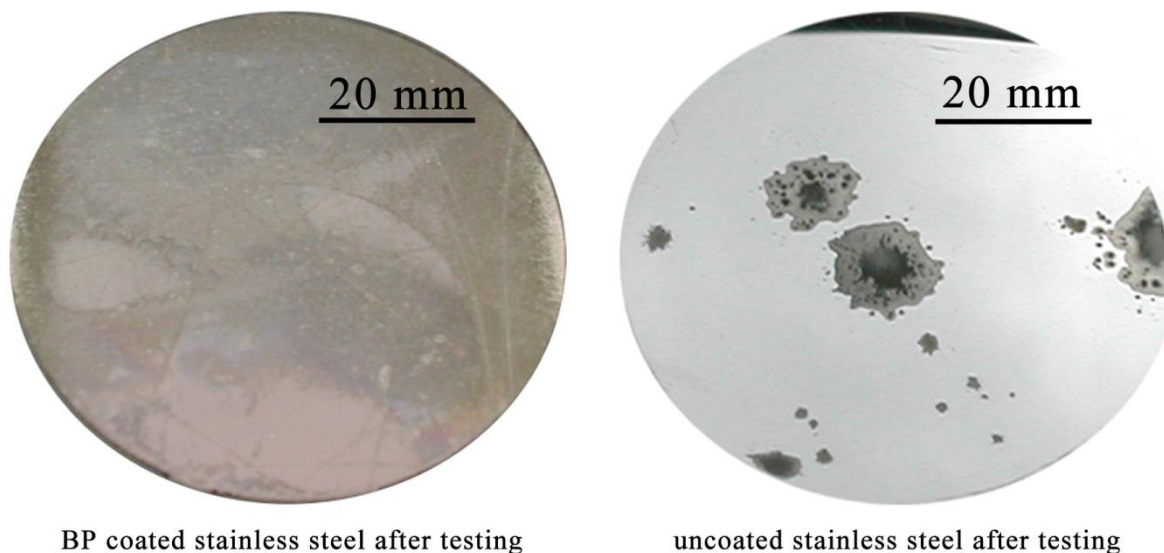
This composition also gives the highest value of polarisation resistance as shown in Fig.9b. The reduction in the double layer capacitance ( $C_{dl}$ ) compared to other film compositions, implies this will

lead to an increase in the contribution to the total electrochemical impedance of the coating surface for the film deposited at  $75 \text{ cm}^3/\text{min}$  flow rate, by an amount given by the capacitive impedance,

$$X_c = \frac{1}{j\omega C} \quad (22)$$

$\omega$  is the frequency,  $j$  is an imaginary number and  $C$  is the double layer capacitance ( $C_{dl}$ ).

Any decrease in the double layer capacitance through a decrease in the polar component of the surface energy, will lead to an increase in the overall electro-chemical impedance of the coating through this contribution. The variation in the pore resistances for all the films investigated with electrochemical impedance spectroscopy (EIS) is as shown in Figs.9c.



BP coated stainless steel after testing

uncoated stainless steel after testing

**Figure 11.** A typical digital camera image of the surface of Boron phosphide coated and uncoated stainless steel substrates after dynamic polarisation from  $-1000\text{mV}$  to  $3000\text{mV}$ . A severe pitting is observed on the uncoated stainless steel substrates.

A summary of the EIS impedances for the coated substrates confirming this observation is shown in the Bode plot in Fig.10. The resistance of the BP coated stainless steel to corrosion after testing in the saline solution is further indicated in the digital camera image in Fig.11. There was no film delamination observed in the BP coated stainless steel after the corrosion tests, as indicated on the digital camera image on the left hand side. The image on the right hand side in Fig.11, which is the uncoated stainless steel, shows severe corrosion degradation. The image on the left hand side of Fig .11 is representative of the surface condition observed on all the films prepared between  $75$  and  $85 \text{ cm}^3/\text{min}$  phosphine flow rate after corrosion testing.

A typical SEM image of the BP coated steel substrate after corrosion testing is shown in fig 12 (left). There was no film delamination observed in this film on the microscopic scale after the corrosion tests as earlier revealed on the macroscopic scale by the digital camera. The crystallites on the surface of the tested films were also identified as NaCl crystals. This investigation reveals that BP films can be used for the corrosion protection of stainless steel in an aggressive saline solution. The results of the OCP measurement, Tafel plots and EIS support this observation. The best corrosion protection was observed for BP films prepared between  $75$  and  $85 \text{ cm}^3/\text{min}$  flow rate of phosphine

during the PECVD process. This observation opens up the potential for using BP films for the corrosion protection of engineering components in saturated saline environments.

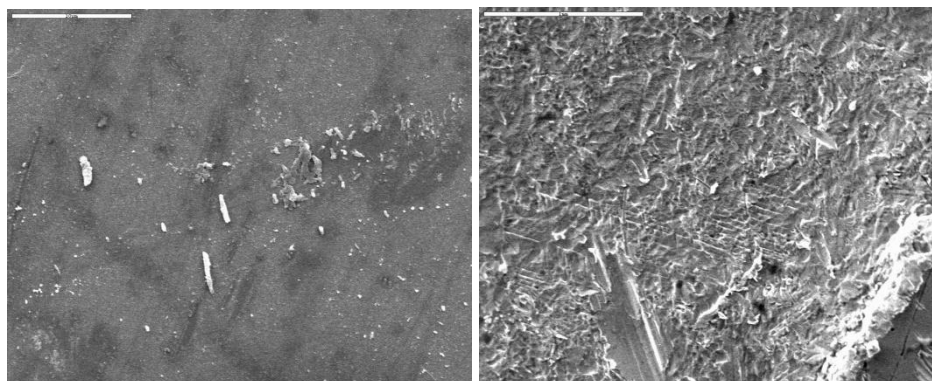


**Figure 12.** SEM images of the surfaces of BP 75  $\text{cm}^3/\text{min}$   $\text{PH}_3$  (left) and uncoated stainless steel substrate (right) after dynamic polarisation from -1000mV to 3000mV.

The observation of a correlation between the surface energy and the corrosion resistance of BP films observed in this investigation further supports similar effects observed in metallic glasses reported by Wang et al, [12] and on super-hydrophobic modified aluminium surfaces by He et al, [14] and Liu et al,[15]. Our observation indicates an opportunity for the potential application of BP films in environments where aqueous corrosion is a major problem, such as in radioactive waste containers[1-3] and in geothermal power plants that use acid-brine steam [9]. The storage of radioactive waste in salt mine repositories or rock-salt vaults, still faces a number of challenges. Amongst these problems is the need for repositories to have a stable geology and the immobilization of waste in a geological repository [28]. Another major problem is with the corrosion of nuclear waste capsule storage material. Sherry and Grimes [29] have highlighted the need for further research into the corrosion protection and degradation of stainless steels, like niobium-stabilized 20124 stainless steel, as container materials for nuclear waste in nuclear waste repositories.

There have been several previous as well as current on-going attempts to identify coatings for improving the performance and storage of nuclear materials. He et al [30] recently proposed SiC coatings for the protection of nuclear graphite material from liquid fluoride salt. Sengupta et al [31] have proposed the use of a graded Ni-YSZ composite coating as a diffusion barrier on Alloy 690 to reduce hazardous nuclear waste inventory. Liu et al [32] previously proposed the use of Co-free Ni-based alloy coatings for improving the wear and corrosion resistance of nuclear valve sealing surfaces. The improved performance of the Co-free Ni-based alloy coatings was associated with the formation of borides and carbides on the nickel alloy surface. Our proposal is that based on the corrosion resistance observed in our investigation and previous reports on the wear and mechanical properties of Boron phosphide coatings [10,11], Boron phosphide coatings can be exploited as potential replacement coatings for many of the above application areas and beyond, with possibly superior performance.

## 6. CONCLUSION

Our investigation on the relationship between surface energy change and corrosion rates in Boron phosphide (BP) films prepared by PECVD, further confirms earlier reports in the literature that a correlation exists between surface energies and corrosion rates in materials in aqueous environments.

We observed that any change in the polar component of the surface energy ( $\gamma^p$ ) will lead to a change in the electrical double layer interaction potential, the zeta potential and the value of the double layer capacitance ( $C_{dl}$ ). Any decrease in the double layer capacitance through a decrease in the polar component of the surface energy, will lead to an increase in the overall electro-chemical impedance of the coating through this contribution.

This is supported by our experimental investigation indicating that the lowest value of the double layer capacitance ( $C_{dl}$ ) of around  $5\mu\text{F}/\text{cm}^2$  occurs for films deposited at the same composition, i.e.  $75\text{ cm}^3/\text{min}$  phosphine flow rate, where the highest contact angle with water and the lowest value of the polar component of the surface energy ( $\gamma^p$ ) was observed. The results of the OCP measurement, Tafel plots and EIS support this observation. The best corrosion protection was observed for BP films prepared between  $75$  and  $85\text{ cm}^3/\text{min}$  flow rate of phosphine during the PECVD process.

Our current experimental investigation demonstrates the potential for using Boron phosphide coatings to protect stainless steel in aggressive brine containing environments like for the steels used in radioactive waste containers in rock-salt formations and in geothermal brine environments. The possibility of varying the surface energy of BP films with phosphine flow rates during deposition also creates an opportunity to use BP films in corrosive environments involving friction, stiction and lubrication.

## References

1. A. Loida, V. Metz, B.Kienzler and H. Geckeis, *Journal of Nuclear Materials*, 346 (2005) 24-31.
2. T. Ahn, H. Jung, X.He and Q. Pensado, *Journal of Nuclear Materials*, 179(2008) 33-41.
3. J. Gimenez, E. Baraj, M.E. Torrero, I. Casas and J. De Pablo. *Journal of Nuclear Materials*, 238(1996) 64-69.
4. N. Mundhenk, P.Huttenloch, T.Kohl, H.Steger and R.Zorn, *Geothermics*, 46(2013) 14-21.
5. N. Mundhenk, P.Huttenloch, B. Sanjuan, T.Kohl, H.Steger and R.Zorn, *Corrosion Science*, 70(2013)17-28.
6. A. Pfening, R. Wiegand, M. Wolf and C.P. Bork, *Corrosion science*, 68( 2013)134-143.
7. E. Hussain, T.N. Narayan, J.J. Taha-Tijerina, S. Vinod, R. Vajtai and P. Ajayan, *ACS applied Materials and interfaces*, 5(2013) 4129-4135.
8. H.W. Hawthorne, A. Neville, T. Troczynski, X.Hu, M. Thammachart, Y. Zie, J. Fu and Q. Yang, *Surface and Coatings Technology*, 176(2004)243-252.
9. T. Sugama , *Materials Letters*, 38(1999) 227-234.
10. A.A. Ogwu, T. Hellwig, D.Haddow, S. Doherty, K. Moellman and F.Placido, *Proc. SPIE- The international society for optical engineering*, Vol. 5786 (2005) 130-136.
11. A.A. Ogwu, T. Hellwig, D.Haddow, S. Doherty, K. Moellman and F.Placido, *Proc. SPIE- The international society for optical engineering*, Vol. 5786 (2005) P365-372.
12. Y.B. Wang, H.F. Li, Y.F. Zheng, S.C. Wei and M. Li, *Applied physics Letters*, 96 (2010)251901-3.
13. S.M. Lee, W.G. Lee, Y.H. Kim and H. Jang, *Corrosion Science*, 63 (2012) 243-252.
14. T. He, Y. Wang, Y. Zhang, Q. Iv, T. Xu and T. Liu, *Corrosion Science* 51(2009) 1757-1761.
15. T .Liu, L. Dong, T. Liu and Y. Yin, *Electrochimica Acta*,55 (2010) 5281-5285.

16. T.H. Muster, A.K. Neufeld, I.S. Cole, *Corrosion Science* 46 (2004) 2337-2354.
17. D.C. Harris, *Materials for infrared Windows and Domes: Properties and performance*, SPIE- The international society of optical engineering (1999)201-202.
18. A.A. Ogwu, E. Bouquerel, O. Ademosu, S. Moh, E. Crossan and F .Placido, , *Metallurgical and Materials Transactions A*, Vol.36A (2005) 2435-2439.
19. J. A. Bryant and A.E. Childress, *Journal of Membrane Science* 203 (2002) 257-273
20. F.M. Fowkes, *J. Adhesion* 4 (1972) 155-167
21. D.K. Owens and R.C. Wendt, *J. Appl. polym.sci* 13(1969) 1741-1747
22. C.J. Van Oss, R.J. Good and M.K. Chaudhry *J. Colloid Surface Sci. III*, (1986)378-390
23. S. Wu: *J. Polymer Sci.* no.34 (1971) 19-30.
24. E.M. Sherif, J.H. Porgieter, J.D. Cummins, L. Cornish, P.A. Olubambi and C.N. Machio, *Corrosion Science*, 51, 2009, 1364-1371.
25. L. Li, Q. Qu, W. Bai, Y. Chen, S. Zhang, G. Gao and Z. Ding, *Int. J. Electrochem. Sci*, 7, 2012, 3773-3786.
26. T. Ohtsuka, *International Journal of Corrosion*, Vol. 2012, 2012, doi: 10.1155/2012 / 915090.
27. M. Chun and I. Lee, *Colloids and Surfaces A: Physico. Eng. Aspects*, 318, 2008, 191-198.
28. A. Mascarelli, are we getting any closer to curing nuclear energy's biggest headache? *Eternal challenge*. *New Scientist*, November 2013, 42-45.
29. A. Sherry and R. Grimes, *The nuclear R & D roadmap*, *Materials World*, September 2013, 32-35.
30. X. He, J. Song, J. Tan, B.Zhang, H. Xia, Z. He, X. Zhou, M. Zhao, X. Liu, L. Xu and S. Bai, *Journal of Nuclear Materials*, 448(2014)1-3.
31. P. Sengupta, D. Rogalia, H. Werner Becker, G. Kumar Dey, S. Chakraborty, *Journal of Hazardous Materials*, 192(2011) 208-221.
32. X. Liu, G. Yu, S.liu, S. Shi, X. He and M. Wang, *Nuclear Engineering and Design*, 241(2011) 4924-4928.